IEEE Access
Multidisciplinary | Rapid Review | Open Access Journal

Received July 28, 2021, accepted August 15, 2021, date of publication August 24, 2021, date of current version September 3, 2021.

Digital Object Identifier 10.1109/ACCESS.2021.3107531

Circularly Polarized Transmitarray Antenna Design Using Meander Line Polarizer for Ku-Band Applications

MUHAMMAD NAEEM IQBAL[1], MOHD FAIRUS MOHD YUSOFF[1], MOHAMAD KAMAL A. RAHIM[1], (Senior Member, IEEE), MOHAMAD RIJAL BIN HAMID[1], ZAHARAH JOHARI[2], AND HAMOOD UR RAHMAN[3]

[1]Advance RF and Microwave Research Group (ARFMRG), School of Electrical Engineering, Universiti Teknologi Malaysia, Johor Bahru, Johor 81310, Malaysia
[2]Faculty of Engineering, School of Electrical Engineering, Universiti Teknologi Malaysia (UTM), Johor Bahru, Johor 81310, Malaysia
[3]Electrical Engineering Department, National University of Sciences and Technology (NUST), Islamabad 44000, Pakistan

Corresponding author: Muhammad Naeem Iqbal (naeem.iqbal@graduate.utm.my)

This work was supported by the Ministry of Higher Education (MOHE) and Ministry of Science, Technology and Innovation (MOSTI), Research Management Centre (RMC), Universiti Teknologi Malaysia (UTM), under FRGS Grant 5F390 and UTMFR Grant 20H79.

ABSTRACT In this paper, a circularly polarized Transmitarray antenna design for the Ku-band frequency range is presented. The transmitarray antenna with 121 elements is designed using a four-layer double square ring with a center patch unit cell. The Unit cell parametric analysis shows a high transmission coefficient magnitude of −1.26 dBi and a wide phase range of 256 degrees. A meander line polarizer is designed at 12GHz to convert the polarization from linear to circular. This meander line polarizer is placed in front of the horn antenna as a superstrate layer. The final measurement results show a high gain circular polarized TA antenna with a maximum gain of 20.17dBic and a value of 1.89 for the axial ratio is achieved at 11.2 GHz. The 1dB antenna gain and 3-dB axial ratio bandwidth are calculated as 0.65GHz and 1.07GHz, respectively. The proposed design offers a low profile and less complex structure, making it suitable for long-range communication systems, especially in Ku band applications.

INDEX TERMS Circular polarization, frequency selective surface, meander line, transmitarray, unit cell.

I. INTRODUCTION

Over the years, there has been an increasing interest in Ku band [1] satellite services, including broadcasting digital TV, radio, and broadband internet [2]. The metallic reflector antennas [3], [4] have mainly been used for satellite applications due to their low manufacturing cost and greater efficiency [5]. Reflectarray antennas have a planar structure and present solutions to bulky size problems of metallic reflector antennas. Low profile and compact reflectarray antennas have also been designed [5]–[8] while fulfilling the high gain requirement. Transmitarray (TA) antennas have gained interest in the last years due to their low profile, zero feed blocking-as in the reflectarray antennas, and spatial feeding to avoid the losses in designing complex matching networks-as in phased array antennas.

The associate editor coordinating the review of this manuscript and approving it for publication was Chinmoy Saha.

Among the different configurations used for designing transmitarrays, the most commonly used are metamaterial, receiver-transmitter, and Frequency Selective Surface (FSS) types. Metamaterial transmitarrays use the principle of changing material properties, i.e., permittivity and permeability, to change the unit cell phase [7], [9]–[11]. Altering the material properties poses a significant challenge in designing this type of transmitarrays. The receiver-transmitter type transmitarrays use interconnected layers through vias and a biasing layer for phase-shifting [12]–[19]. Assembling this type of structure, interconnecting vias, layer alignment, and incorporating active devices in the bias layer increases the design's complexity. On the other hand, FSS type transmitarrays constitute planar multilayer structures to achieve the desired phase range [20]–[24]. Different types of unit cell shapes have been implemented in FSS transmitarrays to increase the bandwidth, reduce the insertion loss, control the beam steering, and adjust the reconfigurability from linear to circular polarization.

Significant works have been done in transmitarray antennas to increase the bandwidth, reduce the insertion loss due to multiple layers involved, and control the beam steering. However, fewer works were reported on dual-polarization or circularly polarized transmitarrays. The few techniques implemented have used the conventional receiver-transmitter configuration, which has the drawbacks of narrow bandwidth and complexity of structure due to interlayer connections through vias. The design in [25] shows the 3-bit unit cell design with circular polarization obtained by the truncating corners technique. However, the sequential rotations of unit cell patches and interconnection vias make the fabrication and assembling process difficult. Another method uses a polarizer with dual-linear elements to implement the circularly polarized transmitarray [26]. Similarly, another design is implemented using sequential and random unit cell rotations in a receiver-transmitter configuration [27].

In this study, a circularly polarized transmitarray antenna is designed using a four-layer FSS unit cell configuration. The unit cell structure consists of a double square ring with a center patch. At first, a linear polarized 11 $\times$ 11 (121 elements) FSS transmitarray antenna is designed. Then, we use the meander line polarizer as a superstrate structure to convert linear polarization to circular polarization. The advantage of this structure is that we can produce high gain TA with minimum insertion loss. This structure also provides a low-profile and less complex design compared to other transformation methods.

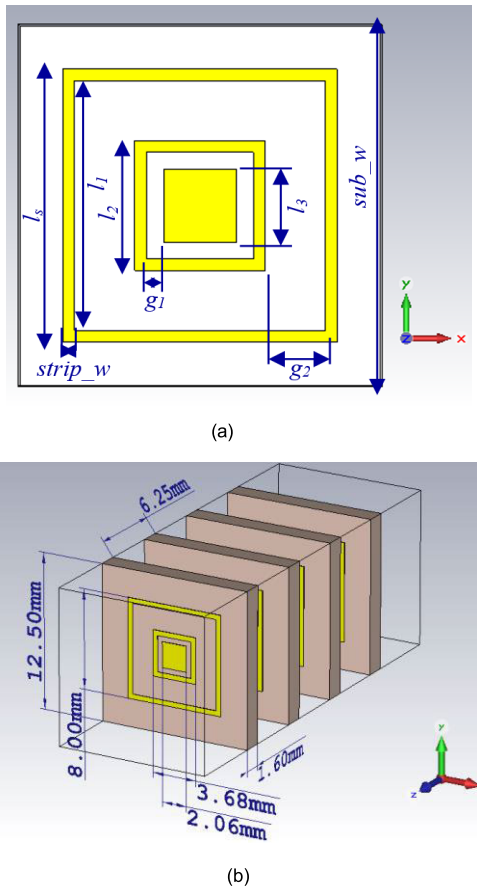

FIGURE 1. (a) Double square ring with center patch structure (b) Four-layer FSS unit cell isometric view.

II. CIRCULARLY POLARIZED TRANSMITARRAY ANTENNA DESIGN

A. TRANSMITARRAY UNIT CELL DESIGN

The frequency selective surface type transmitarray composes of multiple array layers. The transmission coefficient magnitude and phase can be controlled by unit cell parametric variations and interlayer spacing. To design the FSS transmitarray, a novel double square ring with a center patch structure is used, as shown in Figure 1(a). Table 1 depicts the complete dimensions of the unit cell. It is observed that the phase range can be increased by adding the number of FSS layers. In this design, four layers of FR4 substrate with a thickness of 1.6mm have been implemented. The FSS inter-layer spacing is kept at a quarter wavelength, i.e., 6.25mm. Figure 1(b) shows the 3D view of a four-layer structure.

To perform the parametric analysis, the length "l_s" is varied, and the remaining lengths "l_1, l_2, l_3," and gaps "g_1, g_2" vary according to the relations provided in Table 1. The unit cell size is illustrated by the parameter "*sub_w,*" which is kept at 12.5mm, i.e., half of the wavelength at the design frequency of 12GHz. The transmission coefficient magnitude and phase plots by varying the parameter "l_s" can be seen in Figure 2. Results show that the 256 degrees phase range is obtained by varying the length "l_s" from 6.1 to 9.3 mm. The phase range can be increased using a lower permittivity substrate. It can be observed that the phase range has been increased to 501 degrees when the RT Duroid 5880 substrate with relative permittivity of 2.2 is used, as shown in Figure 3. In this case, the length "l_s" is varied from 8.2mm to 12mm.

TABLE 1. FSS transmitarray unit cell dimensions.

Symbol	Description	Values (mm)
sub_w	length of TA unit cell substrate	12.5mm ($\lambda/2$, half of the wavelength at 12GHz)
l_s	the external side length of the outer square ring	6.1mm to 9.3mm
l_1	inner side length of outer square ring	5.3mm to 8.5mm, value = ($l_s - 2 * strip\_w$)
l_2	side length of inner square ring	2.6mm to 4.4mm, value = ($l_1 - 2 * g_1$)
l_3	side length of center patch	1.45mm to 2.45mm, value = ($l_2 - 2 * g_2$)
g_1	gap between the two rings (outer & inner)	1.34mm to 2.05mm, value = ($0.22 * l_s$)
g_2	gap between the inner ring and center patch	0.57mm to 0.96mm, value = ($0.22 * l_2$)
strip_w	width of the Cu strip used in outer and inner rings	0.4mm

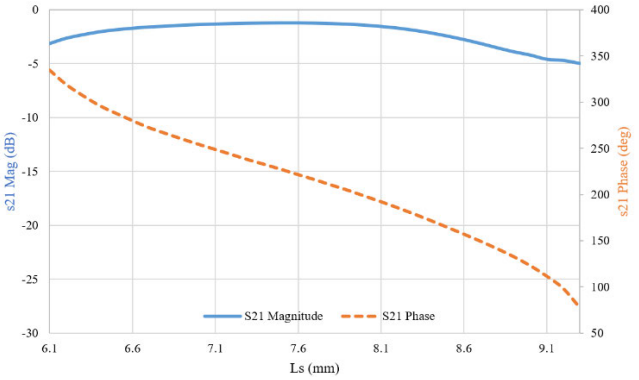

FIGURE 2. Transmission coefficient magnitude and phase plots versus the length l_s for unit cell design using FR4 substrate.

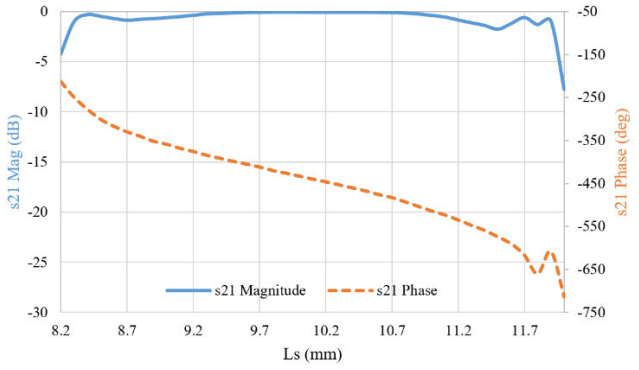

FIGURE 3. Transmission coefficient magnitude and phase plots versus the length for the Rogers RT Duroid 5880 substrate.

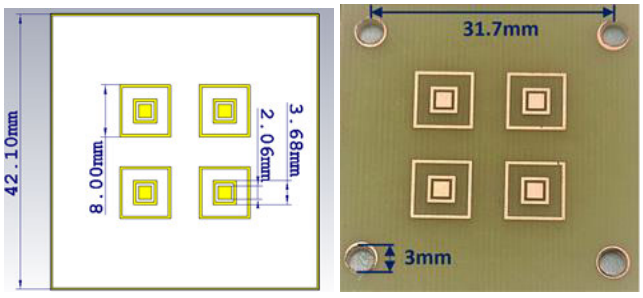

(a) (b)

FIGURE 4. (a) Simulated (b) Fabricated 2 × 2 unit cell prototype using FR4 substrate.

A 2 × 2 unit cell array is fabricated and measured to validate the unit cell simulation results, as shown in Figure 4. Figure 5 shows the measurement setup by using rectangular to square waveguide transitions along with WR90 adaptors. This waveguide transition is needed to accommodate at least 2 × 2 unit cell arrays with similar periodic boundary conditions. Rectangular to square waveguide transitions are fabricated using 3D printing and conducting copper layer pasted on the inner side of waveguide transitions. The transmission coefficient magnitude and phase plots are given

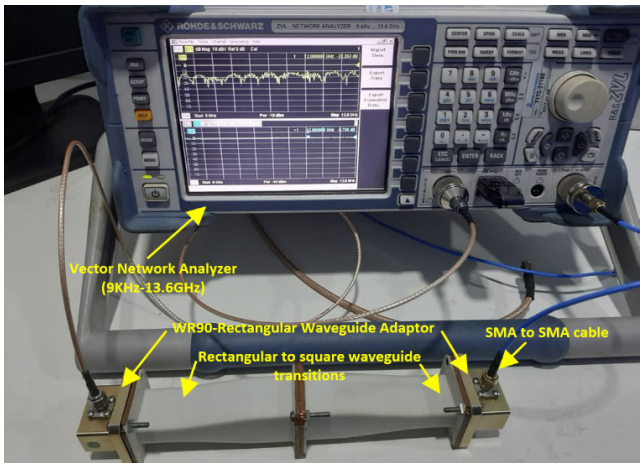

FIGURE 5. Unit cell testing using waveguide transitions with WR90 rectangular waveguide adaptors.

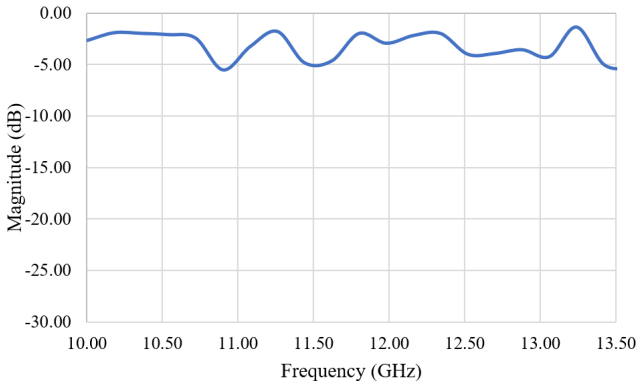

FIGURE 6. Measured S21 magnitude versus frequency plot.

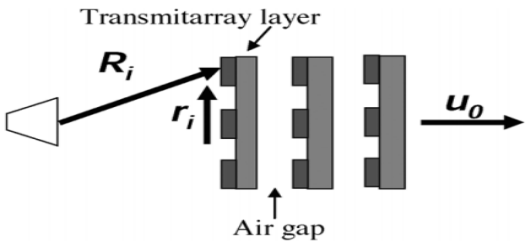

FIGURE 7. Multilayer FSS transmitarray design configuration.

in Figures 6 and 7, respectively. The results show that a good transmission coefficient response has been obtained from 10GHz to 13.5GHz. The magnitude varies from −1.3dB to −5dB, indicating the propagation wave can pass through the FSS layer.

B. FSS TRANSMITARRAY ANTENNA DESIGN

The transmission coefficient magnitude and phase depend on the FSS layers configuration as well as the design structure. Unlike the receiver-transmitter configuration, FSS type transmitarrays do not require the biasing layers for phase shifting. Instead, the phase shift can be controlled individually by

changing the unit cell dimensions. Figure 7 shows the complete transmitarray antenna configuration with multiple FSS layers. Equation (1) is used to calculate the incident phase requirement at each unit cell position [28]. The outgoing transmitted beam from FSS layers is customized to have a zero-degree phase shift for a coherent main beam.

$$\Phi_i + k\,[R_i + r_i.u_0] = 2\pi n, \quad n = 0, 1, 2, \ldots \tag{1}$$

where Φ_i is the phase adjustment value required at each unit cell position, R_i and r_i are the position vectors specifying the location of the unit cell, k is the propagation constant, and u_0 is the direction of the main transmitted beam.

The directive gain of the array antenna depends upon the effective area of the array. By increasing the effective area, directivity also increases, as shown from the plot shown in Figure 8. The number of elements is varied from 4 to 14 elements along each x and y-axis. However, it can be reduced due to the impedance mismatch and feeding losses. In this transmitarray design, an 11 $\times$ 11 element size array is selected to achieve 20dBi gain with keeping the compact size.

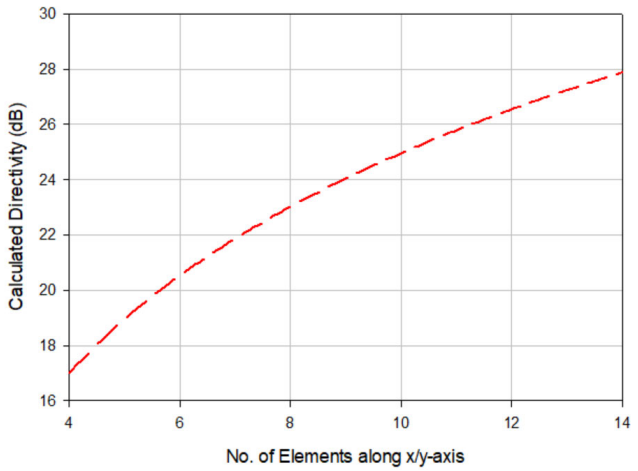

FIGURE 8. Directivity versus the number of elements along x/y-axis for a square-shaped transmitarray.

A four-layer double square ring with a center patch has been implemented as the array elements mentioned earlier. The FSS array structure comprises an 11 $\times$ 11 (121 elements) array with a total size of 162.5mm x 162.5mm, as shown in Figure 9. The unit cell size selection is based on the phase adjustment required at each unit cell position. Compared to other TA feeding sources, such as the microstrip patch antenna, the horn antenna is selected due to its wider bandwidth and higher gain property. In our design, we have used an X-band horn antenna operating over the frequency bands of 8-13.6GHz. The spatial feeding technique has proved to be a better alternative to the previously used complex feeding and power division circuits. The horn antenna gain of 14dBi is achieved from the measurement results. Figures 10(a) and (b) show the final simulated and

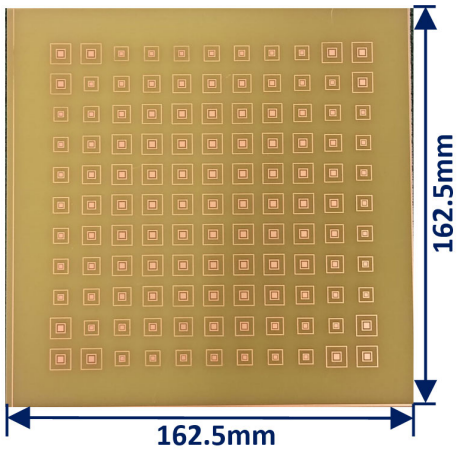

FIGURE 9. Fabricated 121-element FSS transmitarray design.

fabricated TA prototype. An eight-column pillar is assembled using Teflon-based plastic spacers to maintain a fixed spacing between the feeding source and FSS layers. The focal distance (between feed source and FSS layers) is 103.9mm, making the F/D ratio 0.8.

The incident phase for the individual unit cells has been calculated using equation (1). It depends upon the position of the unit cell with respect to the center point of the array and the feeding source. The calculated incident EM wave phase for the 11 $\times$ 11 array has been given in Table 2 below. It can be seen that the phase is varied from 38.16 degrees to a maximum of 345.6degrees. The total phase range required to design the Transmitarray model is 307.44 degrees. The parameter "*ls*" is utilized in designing and phase adjustment for the Transmitarray unit cells. It is varied over the range of 6.1mm to 8.8mm. The optimized design values of the length for each unit cell are mentioned in Table 3.

The measurement S11 results show wide impedance bandwidth of 33.3% from 8GHz to 12GHz, as shown in Figure 11. In the following, Figure 12 depicts the simulated and measured gain results. It can be seen that the measured maximum peak gain has been shifted to a lower frequency at 9.8GHz. This may differ due to the fabrication precision dimensions and alignment errors between each FSS layer and the horn antenna. The 1-dB gain bandwidth is measured as 10%, which is slightly narrow compared to the simulation results (18.3%). However, the peak gain is somewhat increased to 20.4dBi. It can be seen from the parametric studies that variation in inter-layer spacing significantly impacts the antenna peak gain and bandwidth. Thus, causing a gain bandwidth reduction.

Meanwhile, Figure 13 shows the simulated and measured E-plane polar plots for the TA antenna at maximum gain. The results show a good match, especially in the main lobe pattern. The radiation pattern illustrates a pencil beam with a side lobe level less than -10dB and measured 3-dB beamwidth around 18 degrees. The complete three-dimensional radiation patterns can be seen in Figure 14.

TABLE 2. Phase calculation (degrees) for the incident wave for 11 × 11 element array.

Row/Col	Col-1	Col-2	Col-3	Col-4	Col-5	Col-6	Col-7	Col-8	Col-9	Col-10	Col-11
Row-1	103.68	38.16	345.6	307.8	284.4	273.6	284.4	307.8	345.6	38.16	103.68
Row-2	38.16	330.84	273.6	237.6	212.4	205.5	212.4	237.6	273.6	330.84	38.16
Row-3	345.6	273.6	221.76	181.08	156.6	148.32	156.6	181.08	221.76	273.6	345.6
Row-4	307.8	237.6	181.08	139.68	114.4	106.2	114.4	139.68	181.08	237.6	307.8
Row-5	284.4	212.4	156.6	114.4	88.92	80.28	88.92	114.4	156.6	212.4	284.4
Row-6	273.6	205.5	148.32	106.2	80.28	72	80.28	106.2	148.32	205.5	273.6
Row-7	284.4	212.4	156.6	114.4	88.92	80.28	88.92	114.4	156.6	212.4	284.4
Row-8	307.8	237.6	181.08	139.68	114.4	106.2	114.4	139.68	181.08	237.6	307.8
Row-9	345.6	273.6	221.76	181.08	156.6	148.32	156.6	181.08	221.76	273.6	345.6
Row-10	38.16	330.84	273.6	237.6	212.4	205.5	212.4	237.6	273.6	330.84	38.16
Row-11	103.68	38.16	345.6	307.8	284.4	273.6	284.4	307.8	345.6	38.16	103.68

TABLE 3. Double square ring with center patch transmitarray dimension ls(mm) versus array position.

Row/Col	Col-1	Col-2	Col-3	Col-4	Col-5	Col-6	Col-7	Col-8	Col-9	Col-10	Col-11
Row-1	8.7	8.7	6.1	6.3	6.5	6.7	6.5	6.3	6.1	8.7	8.7
Row-2	8.7	6.1	6.7	7.3	7.8	7.9	7.8	7.3	6.7	6.1	8.7
Row-3	6.1	6.7	7.6	8.3	8.6	8.7	8.6	8.3	7.6	6.7	6.1
Row-4	6.3	7.3	8.3	8.8	8.7	8.7	8.7	8.8	8.3	7.3	6.3
Row-5	6.5	7.8	8.6	8.7	8.7	8.7	8.7	8.7	8.6	7.8	6.5
Row-6	6.7	7.9	8.7	8.7	8.7	8.7	8.7	8.7	8.7	7.9	6.7
Row-7	6.5	7.8	8.6	8.7	8.7	8.7	8.7	8.7	8.6	7.8	6.5
Row-8	6.3	7.3	8.3	8.8	8.7	8.7	8.7	8.8	8.3	7.3	6.3
Row-9	6.1	6.7	7.6	8.3	8.6	8.7	8.6	8.3	7.6	6.7	6.1
Row-10	8.7	6.1	6.7	7.3	7.8	7.9	7.8	7.3	6.7	6.1	8.7
Row-11	8.7	8.7	6.1	6.3	6.5	6.7	6.5	6.3	6.1	8.7	8.7

The effect of changing the spacing between FSS layers ''xz_spacing'' is studied. In these simulations, The FSS spacing is varied from 4mm to 10mm with a step size of 2mm. It can be seen in Figure 15 that the impedance is well matched as the S11 values are below −10dB for all four cases. However, by reducing the spacing between TA layers, the peak gain is slightly increased. Figure 16 shows that the peak gain has a maximum value of 19.2dB at 11.5GHz for 4mm spacing. For 6mm, the gain value has been reduced to 18.5dB at 10.7GHz. For 8mm, a peak gain of 18.35dB is

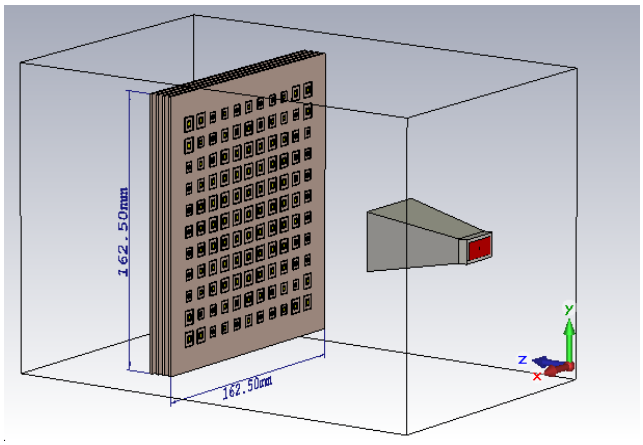

(a)

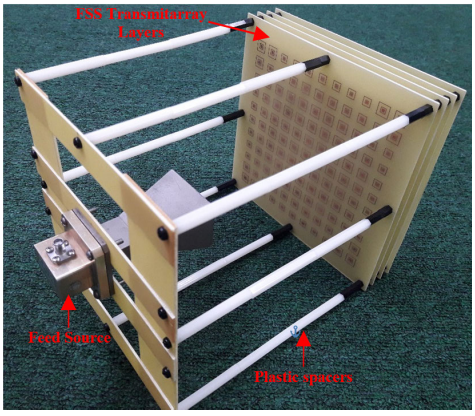

(b)

FIGURE 10. (a) CST simulated model (b) Fabricated TA antenna.

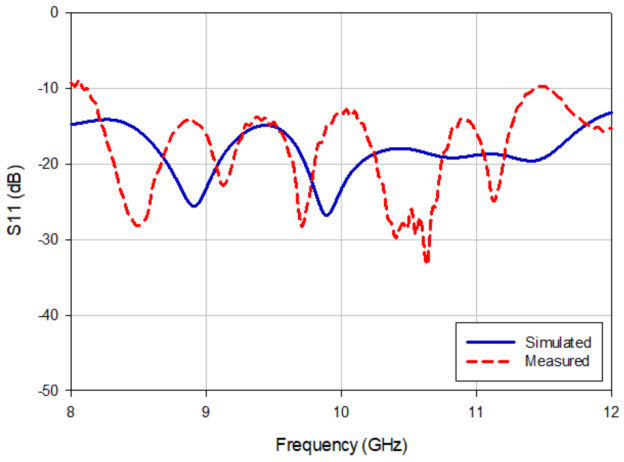

FIGURE 11. S11 simulated and measured results for TA antenna.

obtained at 10.8GHz and further shifted to a 17.7dB peak gain at 10.2GHz for 10mm, respectively. This shows that the maximum gain is reduced and shifted to a lower frequency when the spacing is increased.

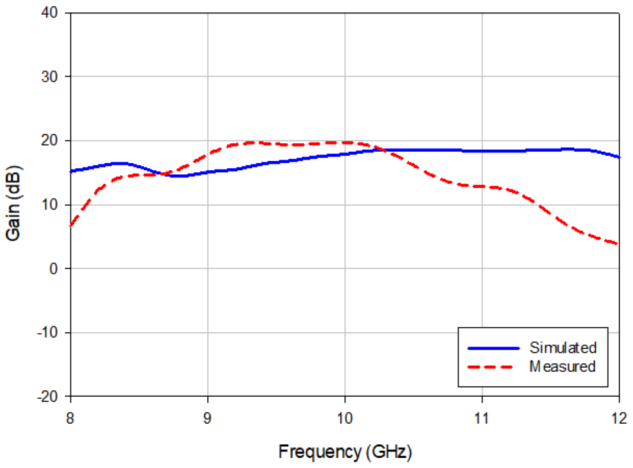

FIGURE 12. Simulated and measured gain versus frequency.

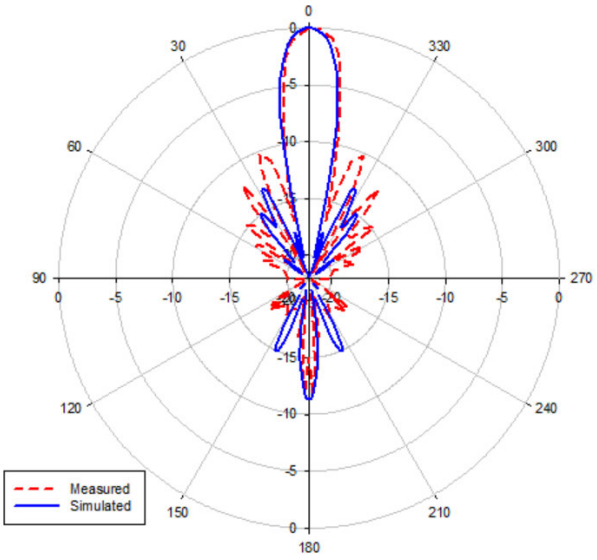

FIGURE 13. E-plane polar plot comparison at maximum gain.

Similarly, the variations of focal distance can also affect the directivity, i.e. the distance between the feeding source and the TA FSS layers. In this study, the focal length is adjusted through parametric simulations. Focal distance is varied from 80mm to 130mm with an F/D ratio varying from 0.615 to a maximum value of 1. Figure 17 shows that the focal length variation less influences the impedance matching and peak gain. The optimum directivity of 18.9dB is obtained for a focal distance equal to 105mm, as shown in Figure 18.

C. LINEAR TO CIRCULAR POLARIZATION USING MEANDER LINE POLARIZER

Many techniques have been used to convert the polarization from linear to circular, LHCP to RHCP, and vice versa. These include using receiver-transmitter structures [14], [25], [27] or using specific FSS unit cells [26], [29]–[31]. However, these techniques have disadvantages due to complex

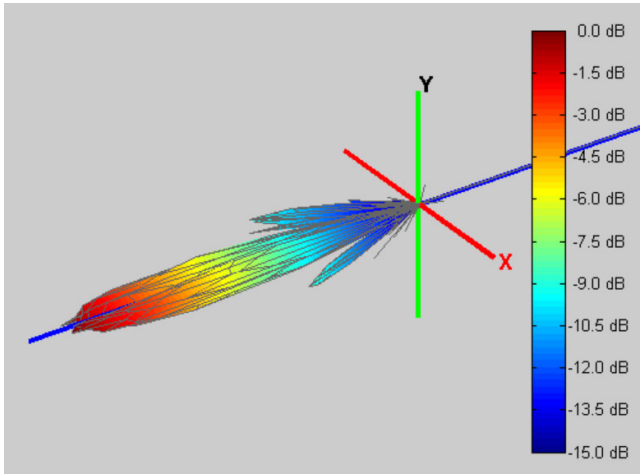

FIGURE 14. The 3D radiation pattern of complete TA antenna at 10.8GHz.

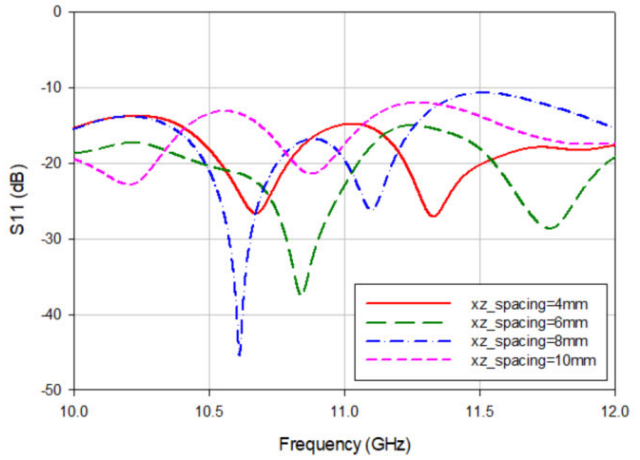

FIGURE 15. Parametric s11 versus frequency plots for different TA layer spacing values.

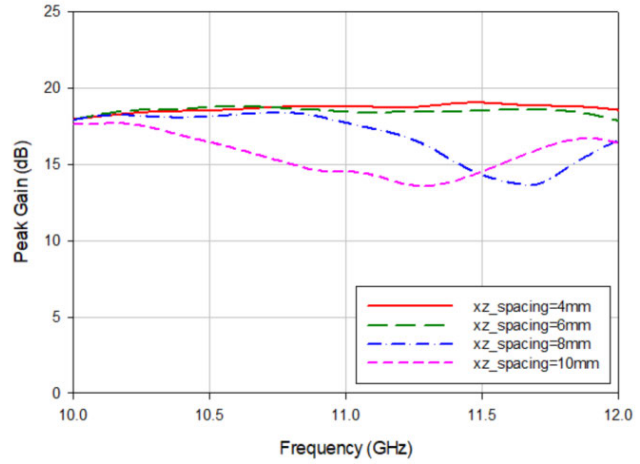

FIGURE 16. Parametric gain versus frequency plots for different TA layer spacing values.

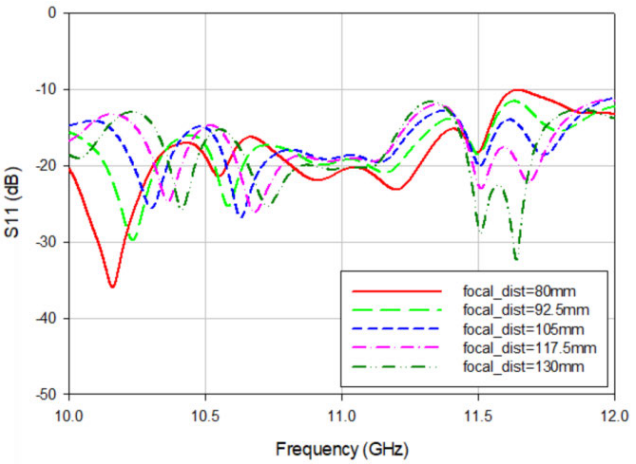

FIGURE 17. Parametric s11 versus frequency plots for different focal distance values.

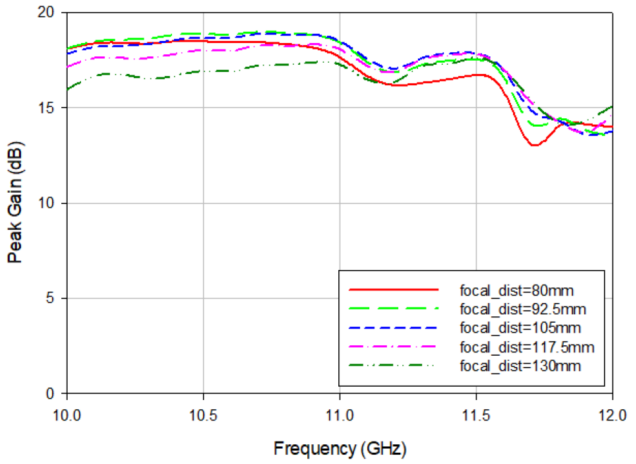

FIGURE 18. Parametric peak gain versus frequency plots for different focal distance values.

structures such as interconnection and biasing circuits. As for the FSS type, it is difficult to have a reconfigurable polarization because of the large number of active devices and controlling/biasing circuits required. Meander line polarizer has been effectively used in microstrip patch antenna designs to convert polarization from linear to circular [32], [33]. However, no reported designs have used this structure in a circularly polarized TA antenna. Therefore, we proposed a simple design using a meander line superstrate structure in front of the horn antenna. Another advantage of this structure is to have reconfigurable polarization by just rotating the superstrate.

Theoretically, the instantaneous electric field for the plane wave at any position can be specified by the equations below.

$$E(z,t) = E_x(z,t)\,\hat{x} + E_y(z,t)\,\hat{y} \tag{2}$$

The components of the E-field at any instant can be described by the equations below.

$$E_x(z,t) = E_x \cos(\omega_t t + \beta_z + \phi_x) \tag{3}$$
$$E_y(z,t) = E_y \cos(\omega_t t + \beta_z + \phi_y) \tag{4}$$

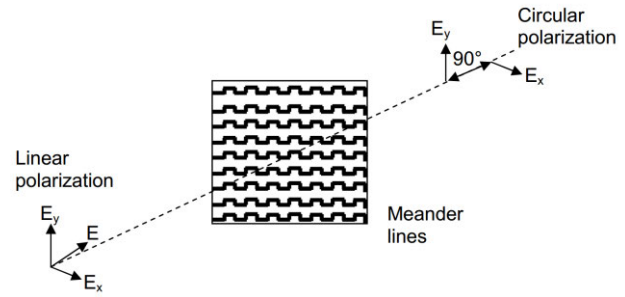

FIGURE 19. Circular polarization definition.

where E_x and E_y show the maximum E-field magnitudes in x and y directions, β_z is the constant of propagation in the z-axis, ω_t shows the angular velocity, ϕ_x and ϕ_y are x and y components of phase angles. For circular polarization, the difference between these phase components can be specified using the equation below.

$$\Delta\phi = \phi_y - \phi_x = \begin{cases} +(2n+1/2)\,\pi & \text{for RHCP} \\ -(2n+1/2)\,\pi & \text{for LHCP} \end{cases} \quad (5)$$

Figure 19 illustrates the basic principle of a meander line polarizer. An incident plane wave with arbitrary polarization direction can be decomposed into two polarization components. One is parallel to the meander line axis (x-component), and the other is perpendicular to the meander line axis (y-component). The meander line structures act differently from these polarization components. For the x-component of the electric field vector, the meander line is equivalent to an inductive element. Whereas for the y-component field, it is equal to a capacitive element. Due to the different reactive effects, the two components have the same output magnitude with a phase difference of 90°. As a result, a CP may be achieved.

The meander line unit cell design and its fabricated prototype are shown in Figure 20. The designs are printed on both sides of the FR4 substrate with a thickness of 1.6mm. The parametric analysis is performed to find optimum values for orthogonal E-field components by getting 90 degrees phase difference. In this configuration, the meander is rotated by 45 degrees from the x-axis to obtain the desired linear to circular polarization conversion. The proposed superstrate is placed at a spacing of 30mm from the front aperture of the feed source.

The optimized meander lines unit cell values are shown in Table 4. Figure 21 shows that for both E_x and E_y vectors, a high transmission coefficient magnitude of −0.37dB and −1.07dB at 12GHz has been achieved, respectively, together with 89.7 degrees phase shift difference. These optimum values are obtained after we have performed a complete parametric study. In these simulations, each defined parameter is varied, including the width of copper strip T1 and T2, the periodic parameters P, S, and the height of element W. The full results are shown in Figure 22 to Figure 25. In the beginning, parameter W was varied from 2 to 4.5mm with

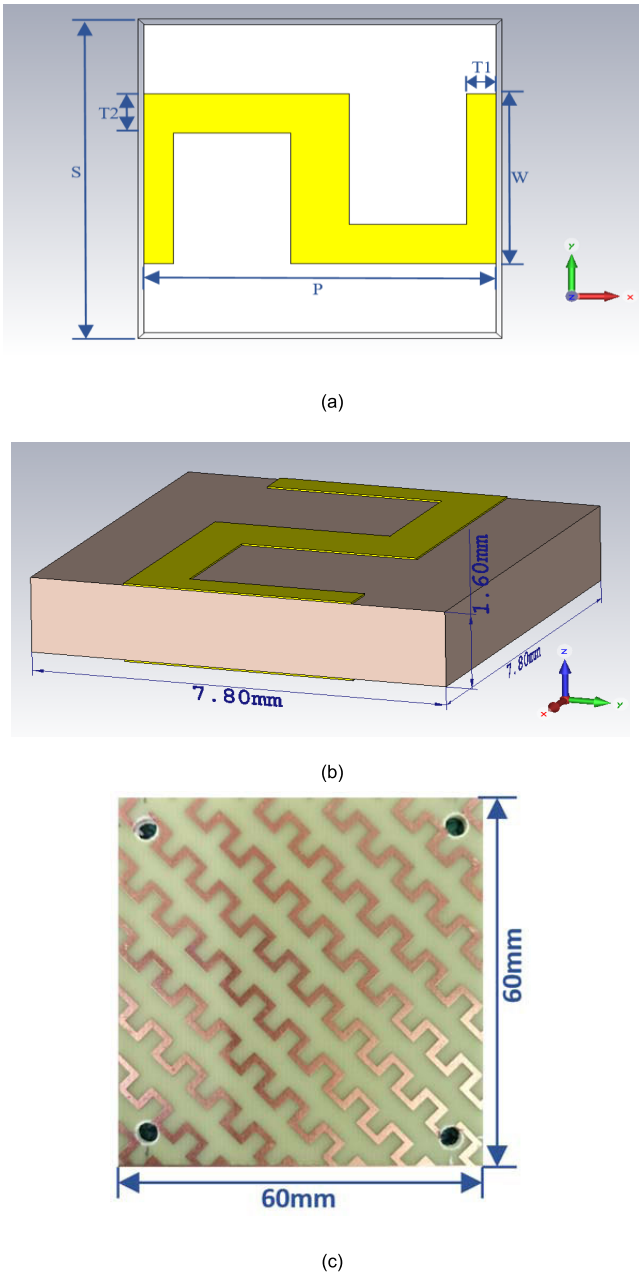

FIGURE 20. (a) Meander line unit cell design using CST (b) Isometric view (c) Polarizer superstrate using meander line.

a 0.5mm step size. As can be seen, the simulation results show that the height (W) has a strong effect on both E_x and E_y transmission coefficient components. It is demonstrated that incrementing the W induces a decrease of the E_x-magnitude, and at the same time, an increase of the E_y-magnitude. As for the transmission phase responses, both simulations show that the E_x and E_y phases increase with higher W.

The second parameter is the T2 strip's widths. The strip's width is varied from 1mm to 1.5mm with a step increment of 0.1mm. The simulation results show that the T2 width variation slightly influences the magnitude and phase of

TABLE 4. Meander line optimized parameter values for 12GHz design.

Symbol	Description	Parametric Analysis Range (mm)	Optimum value (mm)
P	Width of Meander line unit cell	7.2mm to 8.4mm	7.8mm
S	Length of the Meander line unit cell	7.2mm to 8.4mm	7.8mm
T1	Strip width along x-axis	1.2mm to 1.6mm	0.65mm
T2	Strip width along y-axis	1mm to 1.5mm	1mm
W	Height of element	2mm to 4.5mm	4.3mm

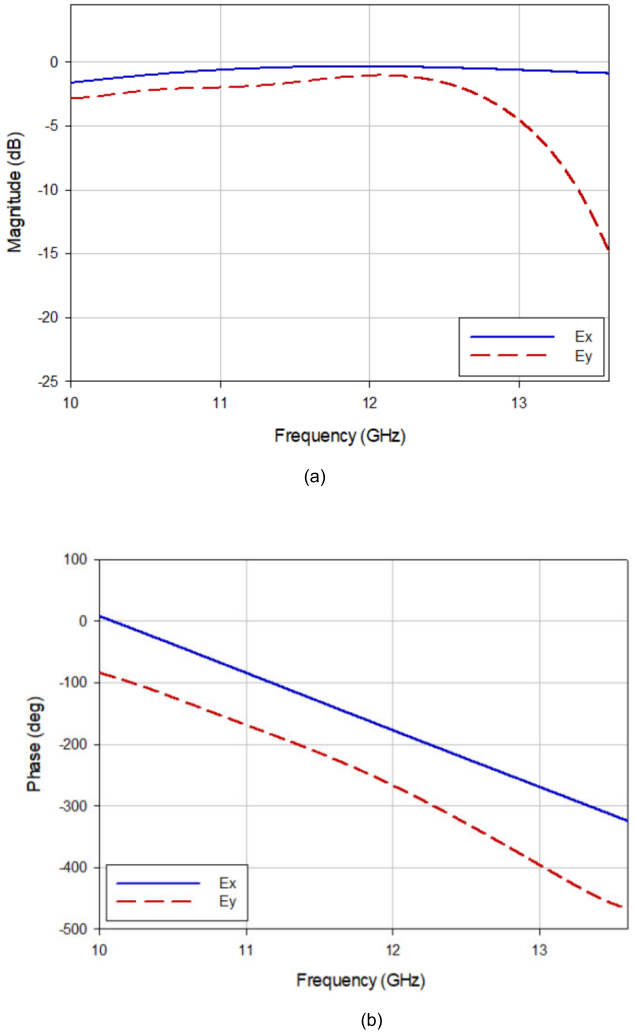

FIGURE 21. Optimized S21 (a) Magnitude (b) Phase plots for 90 degrees phase difference between Ex and Ey configuration unit cells.

the E_x-component. There is only a 24.5-degree phase difference for the E_x-component and 4.3 degrees for the E_y component. In contrast, the magnitude for both components

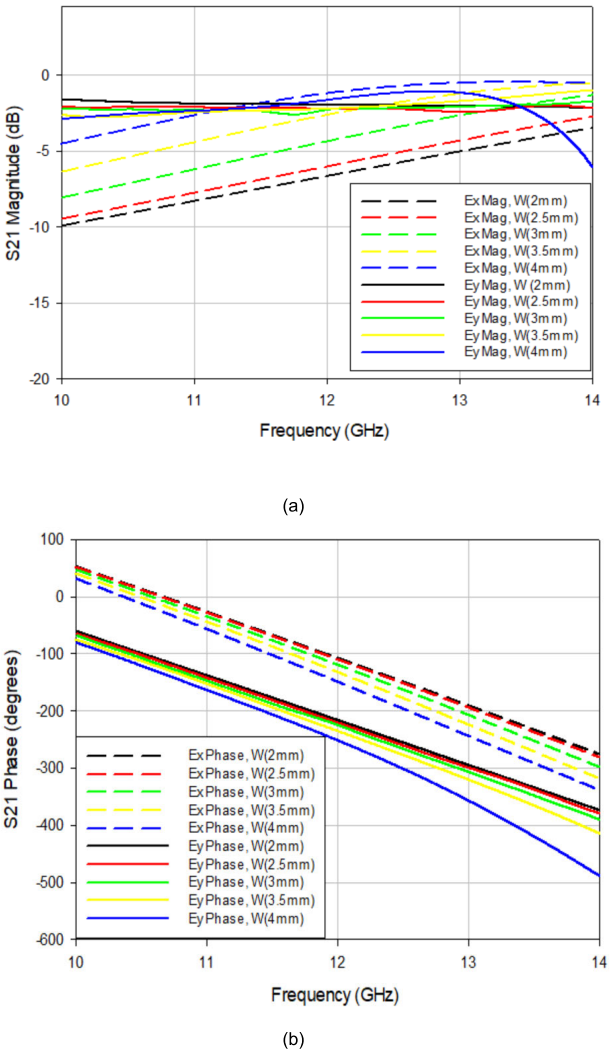

FIGURE 22. Parametric S21 (a) Magnitude (b) Phase plots for parameter "W" variation for Ex and Ey configuration meander line unit cell.

is almost constant for T2 variation. The third parameter is the periodicity (P) of the unit cell. In this simulation, the periodicity is varied from 7.4mm to 8.2mm with a step increment of 0.2mm. The results show that increasing the P periodicity has a minor effect on the E_x and E_y components. It is seen that, for both components, the magnitudes are decreased with larger unit cell periodicity. It has little effect on the transmission phase, with a maximum phase difference of 7.4 degrees. The final parameter to be varied is the meander line strips along the x-axis (T1). The width is varied from 1.2mm to 1.6mm with a step increment of 0.1mm. From these simulation results, the T1 width increment has a negligible effect on magnitudes and phase differences. From Figure 21 to 25, it can also be noticed that the magnitude of Ey is dropped for a higher frequency than 12GHz. The meander line has a narrow passband for Ey component, resulting in a significant increment in axial ratio values for higher frequencies.

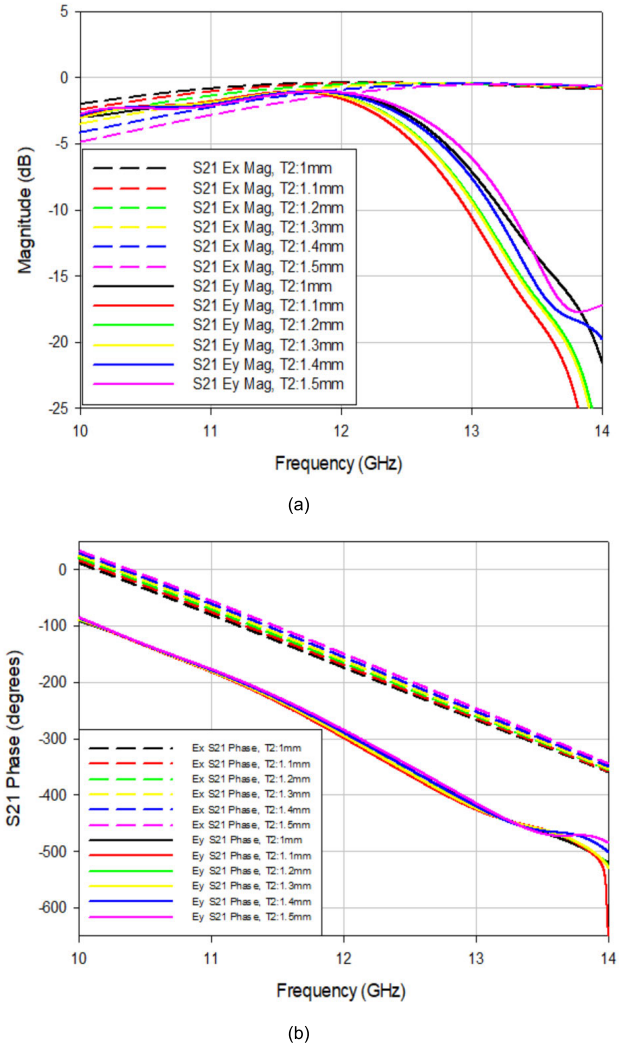

FIGURE 23. Parametric S21 (a) Magnitude (b) Phase plots for parameter "T2" variation for Ex and Ey configuration meander line unit cell.

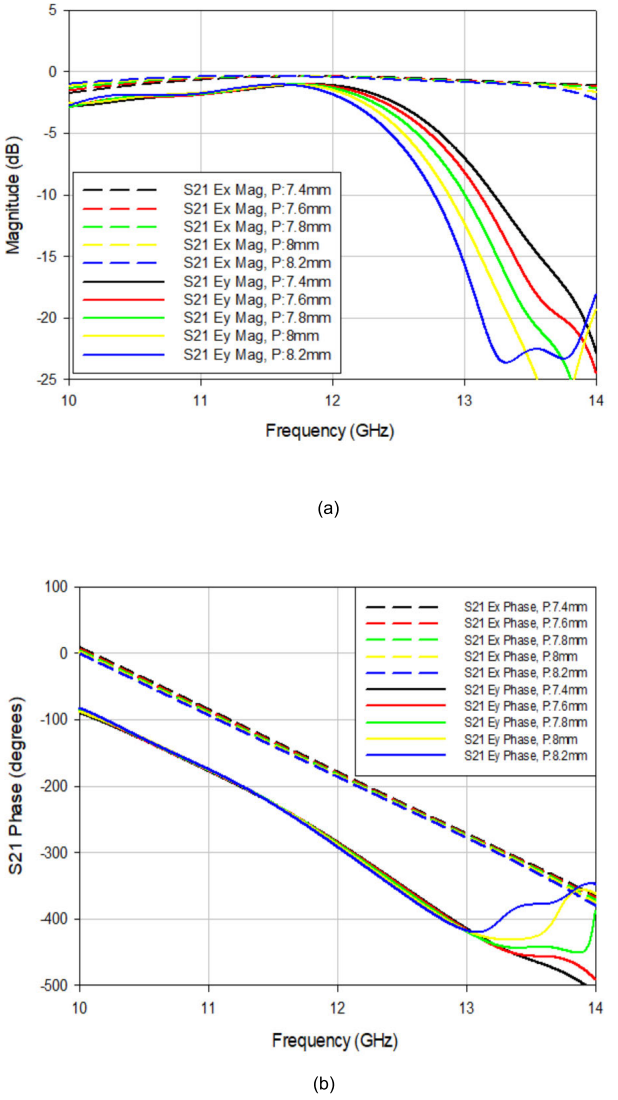

FIGURE 24. Parametric S21 (a) Magnitude (b) Phase plots for parameter "P" variation for Ex and Ey configuration meander line unit cell.

D. CIRCULARLY POLARIZED TRANSMITARRAY ANTENNA DESIGN

This section focuses on designing a circularly polarized FSS transmitarray antenna using a meander line polarizer. The TA consists of a horn antenna as the source, a meander line polarizer, and four-layer FSS transmitarray structures. In this configuration, the meander line polarizer converts the antenna polarization from linear to circular. In the normal position, the meander line polarizer has an anti-clockwise 45-degree rotation about the E-plane and is placed at 23.36mm from the feed source. Simultaneously, the FSS TA layers are placed at a distance of 80.1mm from the polarizer. As a result, a right-handed circular polarized (RHCP) TA has been obtained. Tables 1, 3, 4, and Figure 26 below show the proposed circularly polarised TA design dimensions and the fabricated prototypes.

The measurement setup for radiation pattern, gain, and the axial ratio is shown in Figure 27. The designed TA is mounted as a receiving (RX) antenna. It is rotated by 360 degrees in both the azimuth and elevation planes. The transmitting (Tx) antenna is a double ridged horn rotated in Ex and Ey planes. The axial ratio is calculated as the difference of received power by AUT for Ex and Ey planes, respectively.

The measurement results showed wide impedance matching over the desired frequency range (10GHz - 12.8GHz), as shown in Figure 28. It can be concluded that the inclusion of the polarizer patch has little effect on the impedance matching. In the following, Figure 29 and Figure 30 show the peak gain and the axial ratio plots versus frequency. It can be seen that the measured maximum gain has been shifted to a lower frequency at 10.7GHz. However, the gain is increased to 24dBi when compared with the simulation results. This difference is due to the multilayer alignment precision and fabrication error. The effect of variations in FSS layers spacing on peak gain has been discussed in section B.

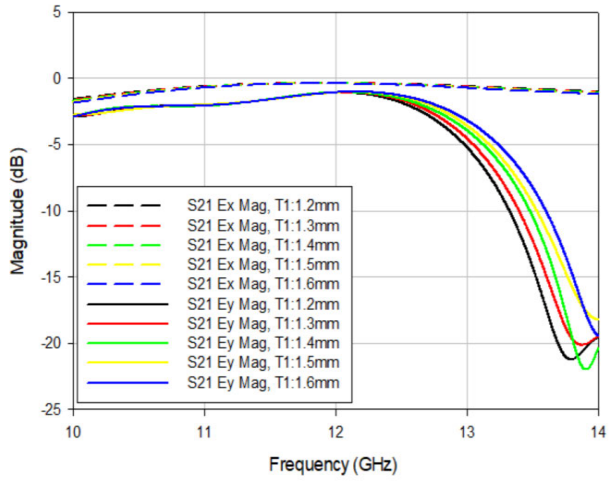

(a)

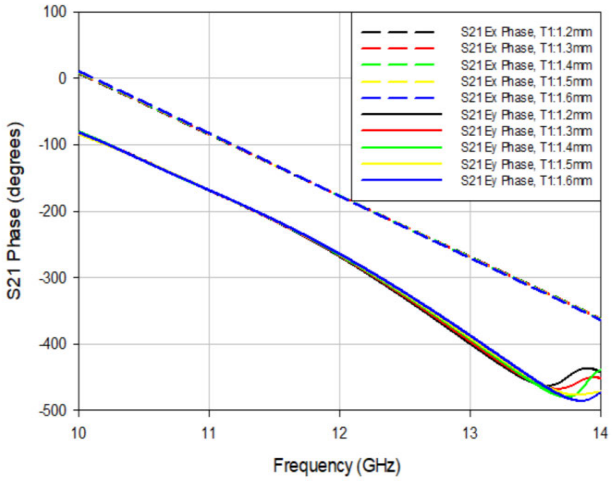

(b)

FIGURE 25. Parametric S21 (a) Magnitude (b) Phase plots for parameter "T1" variation for Ex and Ey configuration meander line unit cell.

In the following, the axial ratio shows a close match between simulated and measured results with three frequency ranges of 11-11.37GHz, 11.7-12GHz, and 12.2-12.4GHz. The measured axial ratio bandwidth is calculated as 0.37GHz, 0.5GHz, and 0.2GHz, respectively. These results proved that the antenna polarization had been successfully converted from linear to circular using the meander line polarizer. Figure 31 shows the polar radiation patterns and the three-dimensional plots at 11.2GHz.

Finally, the effect of the distance between the feeding source and the meander line polarizer is studied. In this simulation, the distance is varied from 12.5mm to 37.5mm with a step size of 6.25mm. Figure 32 shows that better impedance matching is obtained for longer distances. However, this increment will reduce the maximum gain and 1dB gain bandwidth, accompanied by higher axial ratio values, as shown in Figure 33 and Figure 34. Thus, this parametric study needs to be considered in order to optimize the TA design.

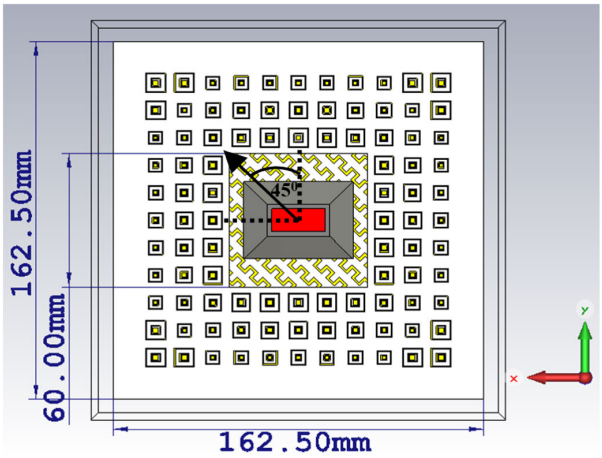

(a)

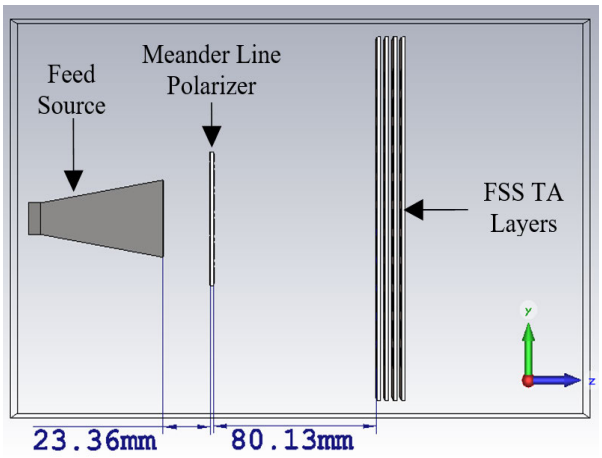

(b)

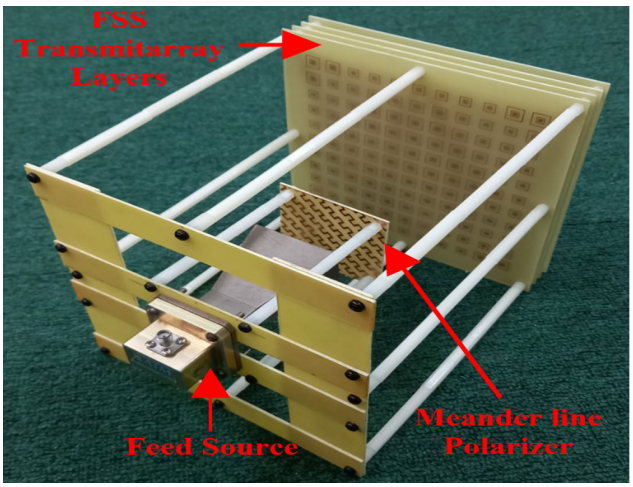

(c)

FIGURE 26. Circularly polarized FSS transmitarray antenna (a) Front-view (b) Side-view (c) 3D view of a fabricated prototype of CP TA.

Table 5 compares this works with different circularly polarized Transmitarray antenna designs using the FSS configuration. It is known that the maximum gain is always dependent

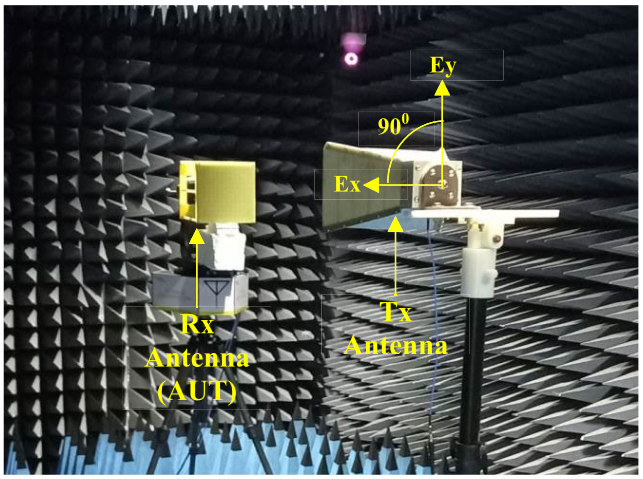

FIGURE 27. Radiation pattern, gain, and axial ratio measurement setup.

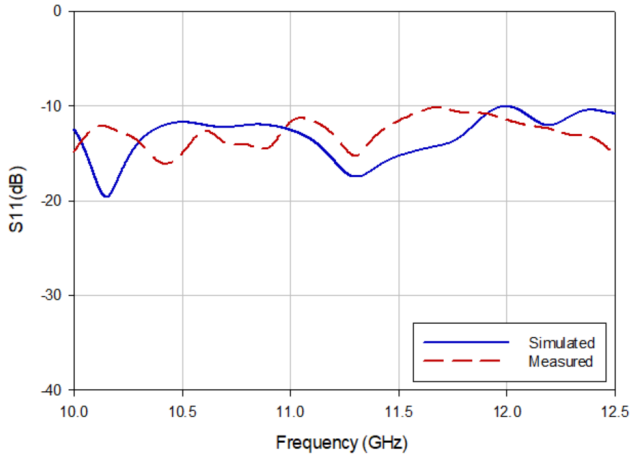

FIGURE 28. S11 simulated and measured results for the CP transmitarray antenna.

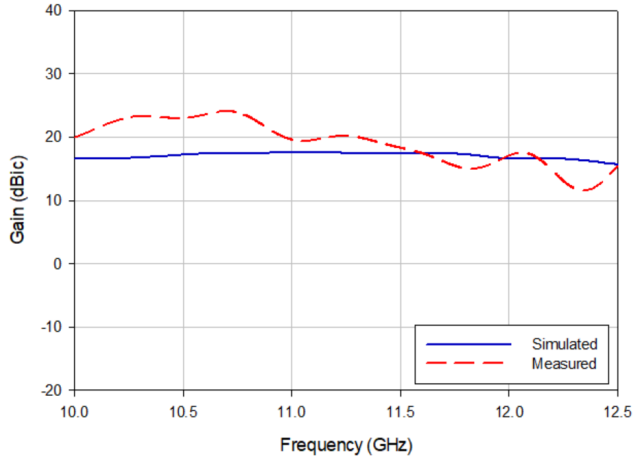

FIGURE 29. Peak gain versus frequency curves for simulation and measurements.

upon the number of elements. The designs are shown in [34] and [36] have a larger number of elements resulting in greater gain value. However, this configuration increases the overall

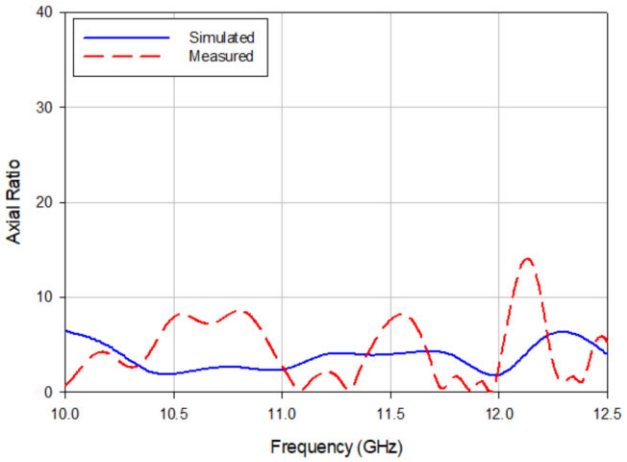

FIGURE 30. Axial ratio versus frequency plots for simulations and measurements.

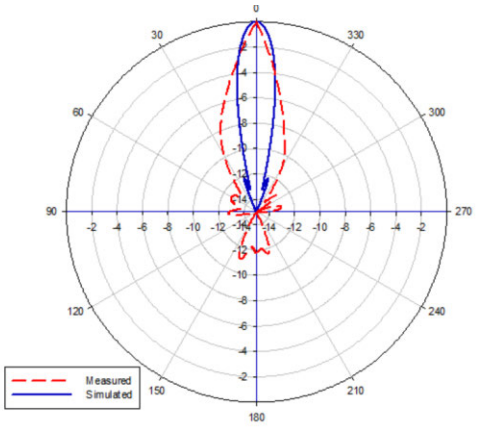

(a)

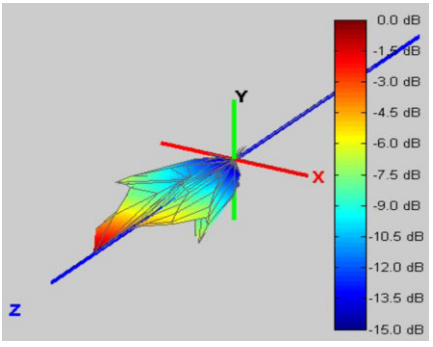

(b)

FIGURE 31. (a) Radiation pattern polar plots at 11.2GHz and (b) 3D radiation patterns at 11.2 GHz.

size of the antenna. On the other hand, our proposed work can produce a high gain value using significantly fewer elements and achieve a lower axial ratio than the design shown in [36] and a greater 3-dB Axial ratio bandwidth than [34] and [26]. Also, it has greater 1-dB gain bandwidth compared to the designs in [26]. In conclusion, we have successfully designed

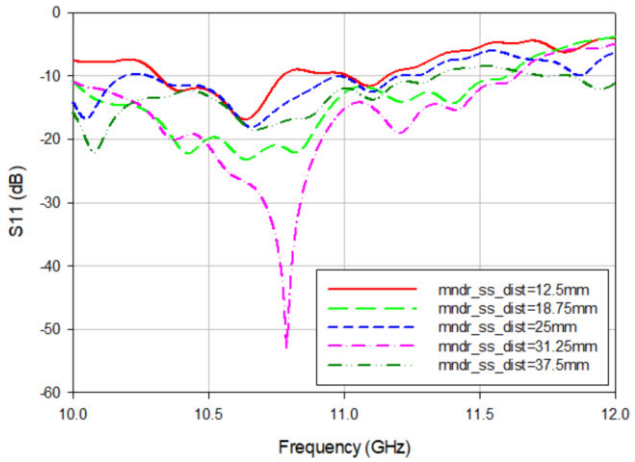

FIGURE 32. Parametric s11 versus frequency plots for different polarizer distance.

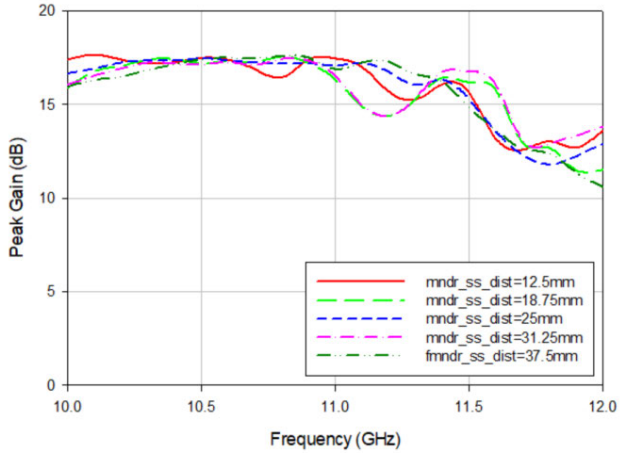

FIGURE 33. Parametric gain versus frequency plots for different polarizer distance.

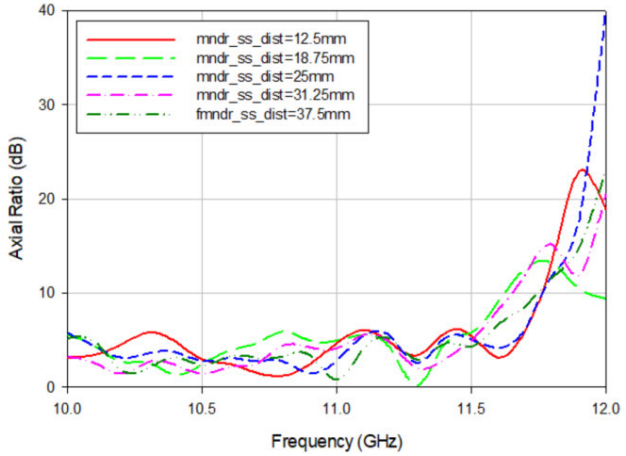

FIGURE 34. Parametric axial ratio versus frequency plots for different polarizer distance.

and showed a new circular polarized TA using the meander line superstrate. This method has produced a low profile and less complex design with higher gain and wider 1-dB bandwidth.

TABLE 5. Comparison of CP TA antenna using FSS configuration.

CP TA Design	Design Frequency (GHz)	Gain (dBic)	1 dB Gain BW, 3 dB AR BW (%)	AR (dB)	Array Size (No. of elements)
[34]	24.6	31.6	5.7, 7.3	0.6	900
[26]	10	21.9	4, 3.5	1.2	341
[35]	10	19.92	13, 24	1	144
[36]	29.5	31.8	7, 10.7	2.9	5513
This work	11.2	20.17	5.4, 8.9	1.89	121

III. CONCLUSION

In summary, a new circular polarization transmitarray antenna by using a meander line polarizer has been presented. Initially, a multilayer unit cell can produce a high transmission coefficient of −1.26 dBi, and a wide phase range of 256 degrees is designed. Then, a linear polarization TA is designed and showed. The maximum gain of 20.4 dBi is obtained. Afterward, we introduce a meander polarizer to convert the polarization from linear to circular. The meander line unit cell parametric analysis is carried out to find the optimum parameters to acquire a low axial ratio. In the final configuration, the meander polarizer substrate is placed in front of the horn antenna. The optimized design is then fabricated and measured. The measured results show that we have successfully achieved a right-handed circular polarized TA antenna with an axial ratio of 1.89 and 20.17 dBic gain at 11.2GHz. The proposed design has the advantages of low profile and compact structure, making it suitable for long-range communication systems for Ku- band applications.

REFERENCES

[1] A. D. Panagopoulos, P.-D. M. Arapoglou, and P. G. Cottis, "Satellite communications at Ku, Ka, and V bands: Propagation impairments and mitigation techniques," *IEEE Commun. Surveys Tuts.*, vol. 6, no. 3, pp. 2–14, 3rd Quart., 2004.

[2] R. V. Gatti, L. Marcaccioli, E. Sbarra, and R. Sorrentino, "Flat array antenna for Ku-band mobile satellite terminals," in *Proc. 5th Eur. Conf. Antennas Propag. (EUCAP)*, 2011, pp. 2618–2622.

[3] Y.-C. Chang and J. Hanlin, "Commercial Ka and Ku bands reflector antennas," in *Proc. IEEE Antennas Propag. Soc. Int. Symp.*, Jun. 2007, pp. 5175–5178.

[4] Y. Rahmat-Samii and A. Densmore, "A history of reflector antenna development: Past, present and future," in *Proc. SBMO/IEEE MTT-S Int. Microw. Optoelectron. Conf. (IMOC)*, Nov. 2009, pp. 17–23.

[5] H. T. Chou, C. Y. Lin, and M. H. Wu, "A high efficient reflectarray antenna consisted of periodic all-metallic elements for the Ku-band DTV applications," *IEEE Antennas Wireless Propag. Lett.*, vol. 14, pp. 1542–1545, 2015.

[6] J. A. Encinar, R. Florencio, M. Arrebola, M. A. S. Natera, M. Barba, J. E. Page, R. R. Boix, and G. Toso, "Dual-polarization reflectarray in Ku-band based on two layers of dipole arrays for a transmit-receive satellite antenna with South American coverage," *Int. J. Microw. Wireless Technol.*, vol. 10, no. 2, pp. 149–159, 2018.

[7] T. Cai, G.-M. Wang, X.-L. Fu, J.-G. Liang, and Y.-Q. Zhuang, "High-efficiency metasurface with polarization-dependent transmission and reflection properties for both reflectarray and transmitarray," *IEEE Trans. Antennas Propag.*, vol. 66, no. 6, pp. 3219–3224, Jun. 2018.

[8] E. Carrasco, J. A. Encinar, and Y. Rahmat-Samii, "Reflectarray antennas: A review," Forum Electromagn. Res. Methods Appl. Technol., Univ. Central Florida, Davenport, FL, USA, Tech. Rep., 2016, vol. 16.

[9] C. Ni, M. S. Chen, Z. X. Zhang, and X. L. Wu, "Design of frequency- and polarization-reconfigurable antenna based on the polarization conversion metasurface," *IEEE Antennas Wireless Propag. Lett.*, vol. 17, pp. 78–81, Jan. 2018.

[10] Y. Zhang, R. Mittra, and W. Hong, "On the synthesis of a flat lens using a wideband low-reflection gradient-index metamaterial," *J. Electromagn. Waves Appl.*, vol. 25, no. 16, pp. 2178–2187, 2011.

[11] Q. Cheng, H. F. Ma, and T. J. Cui, "Broadband planar Luneburg lens based on complementary metamaterials," *Appl. Phys. Lett.*, vol. 95, no. 18, Nov. 2009, Art. no. 181901.

[12] J. Y. Lau and S. V. Hum, "A wideband reconfigurable transmitarray element," *IEEE Trans. Antennas Propag.*, vol. 60, no. 3, pp. 1303–1311, Mar. 2012.

[13] A. Clemente, L. Dussopt, R. Sauleau, P. Potier, and P. Pouliguen, "Design of a reconfigurable transmit-array at X-band frequencies," in *Proc. 15 Int. Symp. Antenna Technol. Appl. Electromagn.*, Jun. 2012, pp. 1–4.

[14] H. Kaouach, L. Dussopt, J. Lanteri, T. Koleck, and R. Sauleau, "Wideband low-loss linear and circular polarization transmit-arrays in V-band," *IEEE Trans. Antennas Propag.*, vol. 59, no. 7, pp. 2513–2523, Jul. 2011.

[15] P. Padilla, A. Muñoz-Acevedo, M. Sierra-Castañer, and M. Sierra-Pérez, "Electronically reconfigurable transmitarray at Ku band for microwave applications," *IEEE Trans. Antennas Propag.*, vol. 58, no. 8, pp. 2571–2579, Aug. 2010.

[16] J. Y. Lau and S. V. Hum, "A low-cost reconfigurable transmitarray element," in *Proc. IEEE Antennas Propag. Soc. Int. Symp.*, Jun. 2009, pp. 1–4.

[17] P. P. de la Torre and M. Sierra-Castañer, "Design and prototype of a 12-GHz transmit-array," *Microw. Opt. Technol. Lett.*, vol. 49, no. 12, pp. 3020–3026, 2007.

[18] H. J. Song and M. E. Bialkowski, "Transmit array of transistor amplifiers illuminated by a patch array in the reactive near-field region," *IEEE Trans. Microw. Theory Techn.*, vol. 49, no. 3, pp. 470–475, Mar. 2001.

[19] D. M. Pozar, "Flat lens antenna concept using aperture coupled microstrip patches," *Electron. Lett.*, vol. 32, no. 23, pp. 2109–2111, Nov. 1996.

[20] C.-Y. Hsu, L.-T. Hwang, T.-S. Horng, S.-M. Wang, F.-S. Chang, and C. N. Dorny, "Transmitarray design with enhanced aperture efficiency using small frequency selective surface cells and discrete Jones matrix analysis," *IEEE Trans. Antennas Propag.*, vol. 66, no. 8, pp. 3983–3994, Aug. 2018.

[21] D. Ferreira, R. Caldeirinha, I. Cuiñas, and T. Fernandes, "Square loop and slot frequency selective surfaces study for equivalent circuit model optimization," *IEEE Trans. Antennas Propag.*, vol. 63, no. 9, pp. 3947–3955, Sep. 2015.

[22] A. H. Abdelrahman, A. Z. Elsherbeni, and F. Yang, "Transmission phase limit of multilayer frequency-selective surfaces for transmitarray designs," *IEEE Trans. Antennas Propag.*, vol. 62, no. 2, pp. 690–697, Feb. 2014.

[23] M. Li, M. A. Al-Joumayly, and N. Behdad, "Broadband true-time-delay microwave lenses based on miniaturized element frequency selective surfaces," *IEEE Trans. Antennas Propag.*, vol. 61, no. 3, pp. 1166–1179, Mar. 2012.

[24] M. Sazegar, Y. Zheng, C. Kohler, H. Maune, M. Nikfalazar, J. R. Binder, and R. Jakoby, "Beam steering transmitarray using tunable frequency selective surface with integrated ferroelectric varactors," *IEEE Trans. Antennas Propag.*, vol. 60, no. 12, pp. 5690–5699, Dec. 2012.

[25] F. Diaby, A. Clemente, K. T. Pham, R. Sauleau, and L. Dussopt, "Circularly polarized transmitarray antennas at Ka-band," *IEEE Antennas Wireless Propag. Lett.*, vol. 17, no. 7, pp. 1204–1208, Jul. 2018.

[26] C. Tian, Y.-C. Jiao, and G. Zhao, "Circularly polarized transmitarray antenna using low-profile dual-linearly polarized elements," *IEEE Antennas Wireless Propag. Lett.*, vol. 16, pp. 465–468, 2016.

[27] L. D. Palma, A. Clemente, L. Dussopt, R. Sauleau, P. Potier, and P. Pouliguen, "Circularly-polarized reconfigurable transmitarray in Ka-band with beam scanning and polarization switching capabilities," *IEEE Trans. Antennas Propag.*, vol. 65, no. 2, pp. 529–540, Feb. 2017.

[28] C. G. M. Ryan, M. R. Chaharmir, J. Shaker, J. R. Bray, Y. M. M. Antar, and A. Ittipiboon, "A wideband transmitarray using dual-resonant double square rings," *IEEE Trans. Antennas Propag.*, vol. 58, no. 5, pp. 1486–1493, May 2010.

[29] H. A. Ghalyon, M. Akbari, and A. Sebak, "A 30 GHz linear-to-circular polarization conversion using two-layer FSS," in *Proc. IEEE Int. Symp. Antennas Propag., USNC/URSI Nat. Radio Sci. Meeting*, Jul. 2017, pp. 671–672.

[30] F. Zhang, G.-M. Yang, and Y.-Q. Jin, "Linear to circular polarization converter with third order meta-frequency selective surfaces," in *Proc. 6th Asia–Pacific Conf. Antennas Propag. (APCAP)*, Oct. 2017, pp. 1–3.

[31] C. Ni, M. S. Chen, Z. X. Zhang, and X. L. Wu, "Design of frequency- and polarization-reconfigurable antenna based on the polarization conversion metasurface," *IEEE Antennas Wireless Propag. Lett.*, vol. 17, pp. 78–81, Jan. 2018.

[32] H. Nakajima, T. Tanaka, M. Takikawa, and N. Yoneda, "A study of meander line polarizer based on equivalent circuits," in *Proc. IEEE Int. Workshop Electromagn., Appl. Student Innov. Competition (iWEM)*, Aug. 2018, p. 1.

[33] F. Greco, E. Arnieri, G. Amendola, L. Boccia, and F. Voci, "Dual band dual circularly polarized antenna with a meanderline polarizer," in *Proc. IEEE Int. Symp. Antennas Propag., USNC/URSI Nat. Radio Sci. Meeting*, Jul. 2018, pp. 119–120.

[34] M. J. Veljovic and A. K. Skrivervik, "Circularly polarized transmitarray antenna for CubeSat intersatellite links in K-band," *IEEE Antennas Wireless Propag. Lett.*, vol. 19, no. 10, pp. 1749–1753, Oct. 2020.

[35] F. Zhang, G. Yang, and Y. Jin, "Low-profile circularly polarized transmitarray for wide-angle beam control with a third-order meta-FSS," *IEEE Trans. Antennas Propag.*, vol. 68, no. 5, pp. 3586–3597, May 2020.

[36] K. T. Pham, A. Clemente, D. Blanco, and R. Sauleau, "Dual-circularly polarized high-gain transmitarray antennas at Ka-band," *IEEE Trans. Antennas Propag.*, vol. 68, no. 10, pp. 7223–7227, Oct. 2020.

MUHAMMAD NAEEM IQBAL received the bachelor's and master's degrees (Hons.) in electrical engineering from the National University of Sciences and Technology (NUST), Pakistan, in 2009 and 2013, respectively. He is currently pursuing the Ph.D. degree in electrical engineering with the Universiti Teknologi Malaysia (UTM). He is also affiliated with the Advanced RF and Microwave Research Group, UTM. During his master's, he performed research on ultra-wideband (UWB) fractal antennas. His research interests include UWB fractal antennas, transmitarray and reflectarray antennas, beamforming, frequency selective surfaces, and polarization converters.

MOHD FAIRUS MOHD YUSOFF received the Bachelor of Engineering degree in electrical-telecommunication and the Master of Electrical Engineering degree in electrical-electronics and telecommunications from University Technology Malaysia, in 2002 and 2005, respectively, and the Ph.D. degree in signal processing and telecommunications from the University of Rennes 1, France, in 2012. He joined UTM, as a Tutor, in 2002. He is currently a Graduate Faculty Member of the Faculty of Electrical Engineering, UTM. His research interests include antenna design, millimeter waves, and microwave devices.

MOHAMAD KAMAL A. RAHIM (Senior Member, IEEE) received the B.Eng. degree in electrical and electronic engineering from the University of Strathclyde, U.K., in 1987, the M.Eng. degree in science from the University of New South Wales Australia, in 1992, and the Ph.D. degree in electrical engineering from the University of Birmingham, U.K., in 2003. From 1987 to 1989, he worked as a Management Trainee with Sime Tyres Mergong Alor Star Kedah and a Production Supervisor with Sime Shoes, Kulim Kedah. He joined the Department of Communication Engineering, Faculty of Electrical Engineering, Universiti Teknologi Malaysia, Kuala Lumpur, as an Assistant Lecturer, in 1989. After receiving his master's, he was appointed as a Lecturer with the Faculty of Electrical Engineering. He was appointed as a Senior Lecturer, in 2005. He was appointed as an Associate Professor with the Faculty. He is currently a Professor of RF and antenna with the Faculty of Electrical Engineering, Universiti Teknologi Malaysia. His research interests include design of dielectric resonator antennas, microstrip antennas, small antennas, microwave sensors, RFID antennas for readers and tags, multifunction antennas, microwave circuits, EBG, artificial magnetic conductors, metamaterials, phased array antennas, computer-aided design for antennas, and design of millimeter frequency antennas.

MOHAMAD RIJAL BIN HAMID received the M.Sc. degree in communication engineering from the Universiti Teknologi Malaysia (UTM), Johor Bahru, Malaysia, in 2001, and the Ph.D. degree from the University of Birmingham, Birmingham, U.K., in 2011. Since 1999, he has been with the Faculty of Engineering, School of Electrical Engineering, UTM. He is currently a Senior Lecturer. His research interests include reconfigurable antenna design for multimode wireless applications.

ZAHARAH JOHARI received the bachelor's degree in electronics, the master's degree in electronics and telecommunication, and the Ph.D. degree from Universiti Teknologi Malaysia, in 2008, 2009, and 2013, respectively. She is currently a Senior Lecturer in electronics with the Universiti Teknologi Malaysia. Her research interests include implementing advanced material such as carbon nanotubes, graphene, and other semiconductor materials in field effect transistor and sensing devices.

HAMOOD UR RAHMAN received the B.Sc. degree in electrical engineering from the University of Engineering and Technology (UET), Lahore, Pakistan, in 1991, the master's degree in electrical engineering from the National University of Science and Technology (NUST), Islamabad, Pakistan, in 1995, and the Ph.D. degree in electrical engineering (RF MEMS/NEMS) from the University of New South Wales (UNSW), Sydney, NSW, Australia, in 2010. Since 2010, he has been working as an Assistant Professor, an Associate Professor, and the Head of the Department of Electrical Engineering, College of Electrical and Mechanical Engineering, NUST, Rawalpindi, Pakistan. He is currently a Visiting Professor with the Centre for Advanced Studies in Engineering, Islamabad. He has authored or coauthored more than 50 publications in journals and conference proceedings. His research interests include the design of microstrip antennas, microwave resonators, and RF transceiver design/characterization.